Hindawi
International Journal of Aerospace Engineering
Volume 2022, Article ID 4696037, 14 pages
https://doi.org/10.1155/2022/4696037

Research Article

Active Control of Aerial Refueling Hose-Drogue Dynamics with the Improved Reel Take-Up System

Jiangfeng Cheng,[1] **Feng Deng**,[1] **Xueqiang Liu**,[1] **and Kang Ji**[2,3]

[1]*College of Aerospace Engineering, Nanjing University of Aeronautics & Astronautics, Nanjing 210016, China*
[2]*Nanjing Engineering Institute of Aircraft Systems, AVIC Jincheng, Nanjing 211106, China*
[3]*Aviation Key Laboratory of Science and Technology on Aero Electromechanical System Integration, Nanjing 211106, China*

Correspondence should be addressed to Jiangfeng Cheng; chengjiangfeng@nuaa.edu.cn

Received 31 May 2022; Accepted 30 June 2022; Published 19 July 2022

Academic Editor: Xingling Shao

An improved reel take-up system for suppressing the aerial refueling hose whipping phenomenon (HWP) is proposed and analyzed. The conventional spring-loaded take-up system is improved by adding a rewinding acceleration changing rate limiter (RACRL), relying on a permanent magnet synchronous motor (PMSM). The effectiveness of this new reel take-up system is confirmed by the numerical simulation at various closure speeds. The results show that the new PMSM-RACRL reel take-up system successfully accomplishes the active control of tension oscillation and the suppressing of HWP with a straightforward strategy. The amplitude of tension oscillation is reduced to one-tenth of that without active control. It is also discovered that the reel take-up speed lagging behind the drogue closure speed is mainly caused by the oscillation of hose tension, and a maximum acceleration of the reel take-up system lower than the maximum closure acceleration of the drogue will inevitably cause the slack and whipping of the hose.

1. Introduction

Over the past decade, rapid developments in artificial intelligence and unmanned aerial vehicle (UAV) technology have seen UAVs become inexpensive and potentially revolutionary air power [1–3]. And aerial refueling techniques serve as a force multiplier for UAVs [4–6], making new missions and capabilities possible [7]. To release the full potential of UAVs, aerial refueling technology becomes the focus of renewed attention. The hose-drogue aerial refueling (HDAR) platform has the advantages of small size, compact and straightforward [8, 9] structure, low manufacturing cost [10, 11], and modular loading/unloading, making it the first choice for autonomous aerial refueling of medium- and large-scale UAVs [12]. However, its deficiency is also apparent. The motion of the drogue is sensitive to atmospheric turbulence, tanker wake, and the receiver bow wave [13–15]. NASA's Dryden Flight Research Center (DFRC) had only achieved success in two of the six docking flight tests in the UAV Autonomous Aerial Refueling Verification Program [7]. It is reported that the US Marine Corps KC-130 series aerial refueling tanker suffered a 2.5% mission failure rate [16]. The main mode of failure is the excessive closure rate of the receiver causes slack and hose whipping phenomenon (HWP) of the hose during hook-up [13]. The HWP generates extreme tension loads on the hose and probe, which may separate the drogue from the probe, even potentially damaging one or both [13, 17]. So it is one of the main causes of failure of refueling after a successful docking, while the reel take-up system is the most effective means to restrain it at present.

Compared with the abundant research on the steady-state trailing hose-drogue refueling system, few studies have been conducted on HWP suppression [18, 19]. Styuart et al. [18] analyzed the dynamic loads on the probe under various motion conditions with reel take-up system malfunction; however, the suppression of HWP had not been studied. Ribbens et al. [19] established a new dynamic model of the hose-drogue system and modeled a gain with a first-order lag controller for suppressing the HWP, but only the two-

dimensional case was analyzed. Ro et al. [14, 15] designed and simulated some conceptual active control strategies for the hose-drogue system during the pre- and the post-hook-up. Vassberg et al. [17, 20–22] studied the modeling for the hose-drogue system and simulated the spring-loaded take-up system work with various conditions based on the KC-10 tanker. Wang et al. [23] proposed and simulated a new active control strategy based on the backstepping method for the HWP. Though the control strategy based on permanent magnet synchronous motor (PMSM) requires more sensors and the control system is more complex [14], the PMSM driver has been widely accepted. To solve the spillover effects caused by truncated models, Liu et al. [8] established flexible hose partial differential equations (PDEs) and proposed a boundary control scheme based on the hose's vibration. Su et al. [24] proposed a PMSM-driven active vibration control scheme for the refueling hose via the robust integral of the sign of the error (RISE) feedback control and extended state observer (ESO). And Zhang et al. [25, 26] proposed unknown input observer-based appointed-time funnel control policy for environmental disturbances and parametric uncertainties. Those control strategy satisfies suppressing the HWP. However, the flexible hose-drogue assembly is still in a critical stable state; it can be seen from the wide range of tension fluctuations. To sum, the spring-loaded take-up system is relatively simple, but it cannot actively adjust the rewinding acceleration of the reel take-up system. On the contrary, the PMSM driver can have good control of the reel take-up acceleration. However, all kinds of control strategies based on PMSM in the existing literature are relatively complex and still fail to achieve good targets of HWP suppression.

In order to achieve the adaptive initiative control of hose tension oscillation and the HWP suppression, a straightforward strategy has been proposed in this paper. Firstly, a finite segment dynamic model of variable-length hose-drogue assembly is built. Secondly, the defect of the spring-loaded take-up system is analyzed. Thirdly, the PMSM is used to replace the spring-loaded to drive the reel; the rewinding acceleration changing rate limiter (RACRL) is proposed and added to improve the take-up system. Finally, the improved PMSM-RACRL reel take-up system response and hose dynamics are simulated within and beyond normal closure speeds.

2. Formulation of Equations of the Variable-Length Finite Segment Model

2.1. Variable-Length Finite Segment Model and Coordinate Systems

2.1.1. Variable-Length Finite Segment Model. The HWP is the main inducement of failure of in-flight refueling during coupling [14, 24]. To suppress this phenomenon, the reel take-up system to tighten the hose in real time is essential. And a variable-length model is a precondition to simulate the recovery strategy of reel take-up systems.

The hose-drogue assembly systems are described by the finite segment (rigid link-ball joint) model. The rigid link is defined as a massless and inextensible cylinder, and the spherical joint is described as a frictionless and lumped mass ball. When considering the take-up function of the reel system, the first link (adjacent to the wing-mount aerial refueling pod) of the hose is treated as a variable-length rod [15]. The second derivative of the length for any link may be expressed as

$$\begin{cases} \ddot{l}_i = -a_{\text{reel}} \ (i = 1), \\ \ddot{l}_i = 0 \qquad\qquad (i = 2, \cdots, n), \end{cases} \tag{1}$$

where a_{reel} is the acceleration of the hose reeling in/out.

For realizing the variable length of the refueling hose, the deployment/retrieval speed or the change rate of hose length is wholly put on the first rod. So the first derivative of the length for any link may be expressed as

$$\begin{cases} \dot{l}_i = -v_{\text{reel}} \quad (i = 1), \\ \dot{l}_i = 0 \qquad (i = 2, \cdots, n), \end{cases} \tag{2}$$

where v_{reel} is the take-up speed of the hose, and the negative sign means its direction is opposite to the $\dot{l}$.

2.1.2. Reference Frames. As depicted in Figure 1, the wing-mount aerial refueling pod is taken as an example. O-XYZ represents an inertial reference frame. The refueling pod is installed on the wing near the wingtip. The motion of hose-drogue assembly during hook-up is deduced by the tow point (hose exit point of the pod) coordinate system O_T-$X_T Y_T Z_T$; it is a right-handed coordinate system. Here, X_T is pointed forward along the trajectory of the tanker, Z_T points in the same direction as the gravitational acceleration, and the Y_T-axis is normal to the $O_T X_T Z_T$ plane. The axes of o_i - $x_i y_i z_i$ and O - XYZ are parallel to the reference frame O_T-$X_T Y_T Z_T$.

2.2. Kinematic Equations. As shown in Figure 2, any link's orientation can be described relative to o_i - $x_i y_i z_i$ using the angles $\theta_{i,1}$ and $\theta_{i,2}$, respectively, relative to the plane o_i $x_i y_i$ and $o_i x_i z_i$. Given the link's length l_i, the link's vector in the tow point coordinate system is as follows:

$$\vec{\mathbf{r}}_i = l_i[-\sin\theta_{i,1} \cos\theta_{i,2}, \cos\theta_{i,1} \cos\theta_{i,2}, \sin\theta_{i,2}]. \tag{3}$$

Then, the vector relation between joint p_{i-1} and p_i in the towing point coordinate system O_T - $X_T Y_T Z_T$ is

$$\vec{\mathbf{p}}_\mathbf{i} = \vec{\mathbf{p}}_{\mathbf{i-1}} + \vec{\mathbf{r}}_\mathbf{i}, \tag{4}$$

where $\vec{\mathbf{p}}_\mathbf{i}$ and $\vec{\mathbf{p}}_{\mathbf{i-1}}$ represent the position vectors of joint p_i and p_{i-1}, respectively.

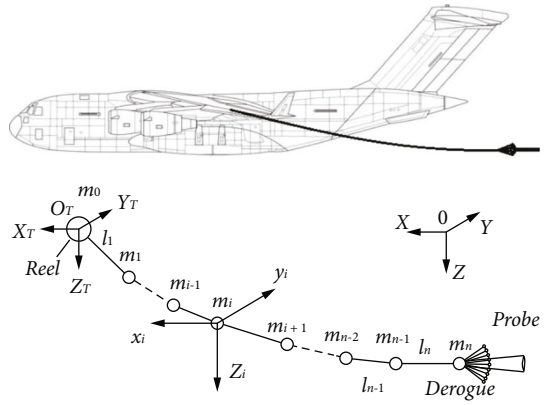

Figure 1: Coordinate systems and hose-drogue model during hook-up.

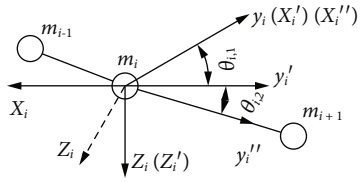

Figure 2: Rigid link's vector and tow point coordinate.

The velocity and acceleration relations between any adjacent joints may be found by differentiating equation (4):

$$\begin{cases} \vec{\mathbf{v}}_{\mathbf{i}} = \vec{\mathbf{v}}_{\mathbf{i-1}} + \dot{\vec{\mathbf{r}}}_{\mathbf{i}}, \\ \vec{\mathbf{a}}_{\mathbf{i}} = \vec{\mathbf{a}}_{\mathbf{i-1}} + \ddot{\vec{\mathbf{r}}}_{\mathbf{i}}, \end{cases} \tag{5}$$

where the derivatives of $\vec{\mathbf{r}}_{\mathbf{i}}$ may be expressed as

$$\dot{\vec{\mathbf{r}}}_{\mathbf{i}} = \sum_{k=1}^{2}\left(\vec{\mathbf{r}}_{\mathbf{i},\boldsymbol{\theta}_{i,k}}\dot{\theta}_{i,k}\right) + \vec{\mathbf{r}}_{\mathbf{i},\mathbf{l}_i}\dot{l}_i + \left(\vec{\boldsymbol{\omega}}_{\mathbf{e}} \times \vec{\mathbf{r}}_{\mathbf{i}}\right), \tag{6}$$

$$\ddot{\vec{\mathbf{r}}}_{\mathbf{i}} = \sum_{k=1}^{2}\left(\vec{\mathbf{r}}_{\mathbf{i},\boldsymbol{\theta}_{i,k}}\ddot{\theta}_{i,k} + \dot{\vec{\mathbf{r}}}_{\mathbf{i},\boldsymbol{\theta}_{i,k}}\dot{\theta}_{i,k}\right) + \dot{\vec{\mathbf{r}}}_{\mathbf{i},\mathbf{l}_i}\dot{l}_i + \vec{\mathbf{r}}_{\mathbf{i},\mathbf{l}_i}\ddot{l}_i + \left(\vec{\boldsymbol{\alpha}}_{\mathbf{e}} \times \vec{\mathbf{r}}_{\mathbf{i}}\right) + \left(\vec{\boldsymbol{\omega}}_{\mathbf{e}} \times \dot{\vec{\mathbf{r}}}_{\mathbf{i}}\right), \tag{7}$$

where $\vec{\boldsymbol{\omega}}_{\mathbf{e}}$ and $\vec{\boldsymbol{\alpha}}_{\mathbf{e}}$ represent the tanker angular velocity (rad/s) and angular acceleration (rad/s^2), respectively.

Assuming that the tanker flight is straight in its direction, the angular motions of the tanker are all zero. Noting that $\vec{\mathbf{r}}_{i,\theta_{i,1}} \cdot \vec{\mathbf{r}}_{i,\theta_{i,2}} = 0$ and taking the product of equation (7) with $\vec{\mathbf{r}}_{i,\theta_{i,k}}$ $(k = 1, 2)$, the second derivative of the orientation angles for any link can be expressed as

$$\ddot{\theta}_{i,k} = \frac{\vec{\mathbf{r}}_{i,\theta_{i,k}} \cdot \left[\vec{\mathbf{a}}_{\mathbf{i}} + \vec{\mathbf{a}}_{\mathbf{i-1i-1}} - \sum_{k=1}^{2}\dot{\vec{\mathbf{r}}}_{i,\theta_{i,k}}\dot{\theta}_{i,k} + \dot{\vec{\mathbf{r}}}_{i,l_i}\dot{l}_i + \vec{\mathbf{r}}_{i,l_i}\ddot{l}_i\right]}{\left(\vec{\boldsymbol{r}}_{i,\theta_{i,k}} \cdot \vec{\boldsymbol{r}}_{i,\theta_{i,k}}\right)} \quad (k = 1, 2). \tag{8}$$

Noting that $\vec{\boldsymbol{r}}_{i,l_i} \cdot \vec{\boldsymbol{r}}_{i,\theta_{i,k}} = 0$, expand equation (8) and substitute equation (2), so the kinematic equations can be obtained as

$$\begin{cases} \ddot{\theta}_{i,1} = \dfrac{\left(\vec{\boldsymbol{a}}_{\boldsymbol{i}} - \vec{\boldsymbol{a}}_{\boldsymbol{i\text{-}1}}\right)}{l_i \cos^2\theta_{i,2}}\dfrac{\partial\vec{\boldsymbol{n}}_{ii}}{\partial\theta_{i,1}} + 2\dot{\theta}_{i,1}\dot{\theta}_{i,2}\tan\theta_{i,2} - \dfrac{2\dot{l}_i\dot{\theta}_{i,1}}{l_i}, \\ \ddot{\theta}_{i,2} = \dfrac{\left(\vec{\boldsymbol{a}}_{\boldsymbol{i}} - \vec{\boldsymbol{a}}_{\boldsymbol{i\text{-}1}}\right)}{l_i}\dfrac{\partial\vec{\boldsymbol{n}}_{\boldsymbol{i}}}{\partial\theta_{i,2}} - \dot{\theta}^2_{i,1}\sin\theta_{i,2}\cos\theta_{i,2} - \dfrac{2\dot{l}_i\dot{\theta}_{i,2}}{l_i}. \end{cases} \tag{9}$$

Given the accelerations of the lumped mass joints, the orientation angles of each link can be solved.

2.3. Kinetic Equations. The relationship between the link vector and the link length according to equation (3) can be expressed as follows:

$$\vec{\mathbf{r}}_i^{\,2} = l_i^2. \tag{10}$$

Substitute equation (5) into the second derivative of equation (10) to get the constraint equation:

$$\left(\vec{\mathbf{a}}_{\mathbf{i}} - \vec{\mathbf{a}}_{\mathbf{i-1}}\right) \cdot \vec{\mathbf{r}}_i + \dot{\vec{\mathbf{r}}}_i^{\,2} = \dot{l}^2_i + l_i \cdot \ddot{l}_i. \tag{11}$$

According to Newton's second law, the acceleration of joint i-th may be expressed as

$$\vec{\mathbf{a}}_{\mathbf{i}} = \begin{cases} \dfrac{\left(-\vec{\mathbf{T}}_i + \vec{\mathbf{T}}_{i+1} + \sum\vec{\mathbf{F}}_i\right)}{m_i} & (i = 1, \cdots, n-1), \\ \vec{\mathbf{a}}_{\mathbf{n}} & (i = n), \end{cases} \tag{12}$$

where $\vec{\mathbf{a}}_{\mathbf{n}}$ is the engagement acceleration of a receiver, and it is also regarded as the acceleration of the drogue approaching the tanker during a hook-up.

Given $\dot{\vec{\mathbf{n}}}_{\mathbf{i}} \times \vec{\mathbf{n}}_{\mathbf{i}} = 0$ and $\vec{\mathbf{n}}_{\mathbf{i}} \times \vec{\mathbf{n}}_{\mathbf{i}} = 1$, let the tension of the i-th link be expressed as $\vec{T}_i = \vec{n}_i \cdot t_i$, and the tension matrix is obtained after simplification:

$$\begin{cases} -\dfrac{1}{m_1}t_1 + \dfrac{\vec{\mathbf{n}}_1 \times \vec{\mathbf{n}}_2}{m_1}t_2 = \left(\vec{\mathbf{a}}_0 - \dfrac{\sum\vec{F}_1}{m_1}\right) \cdot \vec{\mathbf{n}}_1 - l_1 \cdot \dot{\vec{\mathbf{n}}}_1^{\,2} - \ddot{l}_1 \\ \dfrac{\vec{\mathbf{n}}_{i-1} \times \vec{\mathbf{n}}_i}{m_{i-1}}t_{i-1} - \left(\dfrac{1}{m_{i-1}} + \dfrac{1}{m_i}\right)t_i + \dfrac{\vec{\mathbf{n}}_i \times \vec{\mathbf{n}}_{i+1}}{m_i}t_{i+1} = \left(\dfrac{\sum\vec{F}_{i\text{-}1}}{m_{i-1}} - \dfrac{\sum\vec{F}_i}{m_i}\right) \cdot \vec{\mathbf{n}}_i - l_i \cdot \dot{\vec{\mathbf{n}}}_i^{\,2}, \\ \dfrac{\vec{\mathbf{n}}_{n-1} \times \vec{\mathbf{n}}_n}{m_{n-1}}t_{n-1} - \dfrac{1}{m_{n-1}}t_n = \left(\dfrac{\sum\vec{\mathbf{F}}_{n-1}}{m_{n-1}} - \vec{\mathbf{a}}_n\right) \cdot \vec{\mathbf{n}}_n - l_n \cdot \dot{\vec{\mathbf{n}}}_n^{\,2}, \end{cases} \tag{13}$$

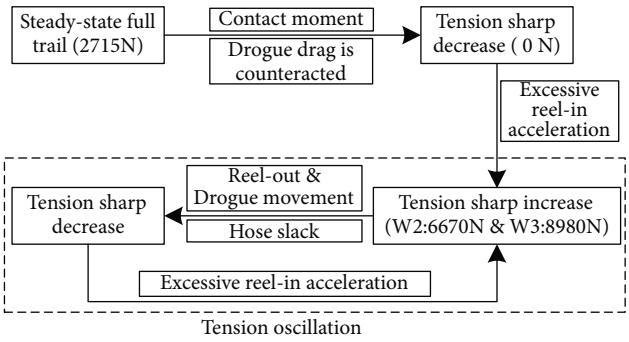

Figure 3: Spring-loaded take-up system and tension oscillation.

Table 1: Uniform flowfield.

Component	Configuration
Altitude (m)	7620
Mach number	0.63
Q (dynamic pressure), Pa	10527

where $\vec{\mathbf{a}}_0$ is the acceleration of the tanker relative to the towing point coordinate system O_T - $X_T Y_T Z_T$.

2.4. External Force. Each segment's weight is equally concentrated at the adjacent lumped mass joints in the variable-length finite segment model. And half of the aerodynamic load of each rigid link is divided evenly to the joints too. Due to the hose's bending, there is a restoring moment on the adjacent links, which tend to restore links coaxial. The moment may be simplified to an external restoring force, imposed on the middle joint between the adjacent links. Therefore the external force (including aerodynamic, weight, and restoring force) of any link may be expressed as

$$\sum \vec{\mathbf{F}}_i = \begin{cases} \dfrac{\left(\vec{\mathbf{D}}_\mathbf{i} + \vec{\mathbf{D}}_\mathbf{i+1}\right)}{2} + \vec{\mathbf{R}}_\mathbf{i} + \dfrac{(m_i + m_{i+1})\vec{\mathbf{g}}}{2} & (i = 1, \cdots, n-1), \\ \dfrac{\vec{\mathbf{D}}_\mathbf{i}}{2} + \dfrac{m_i \vec{\mathbf{g}}}{2} + \vec{\mathbf{D}}_\mathbf{drogue} + m_{drogue}\vec{\mathbf{g}} & (i = n), \end{cases} \tag{14}$$

where $\vec{\mathbf{R}}_\mathbf{i}$ and $m_i = \rho(l_i + l_{i+1})/2$ are the restoring force and the lumped mass of the i-th joint, respectively. And $\vec{\mathbf{g}}$ is the gravitational acceleration. $\vec{\mathbf{D}}_\mathbf{drogue}$ and m_{drogue} are the drag and mass of the drogue, respectively. $\vec{\mathbf{D}}_\mathbf{i}$ is the aerodynamic force of the i-th link, which represents the sum of pressure and skin frictional drag:

$$\vec{\mathbf{D}}_\mathbf{i} = \vec{\mathbf{D}}_\mathbf{i,Pressure} + \vec{\mathbf{D}}_\mathbf{i,\,Skin\quad Friction}. \tag{15}$$

Table 2: Hose, drogue, and reel characteristics.

Component	Configuration
Hose	
Diameter (internal) (cm)	5.08
Diameter (external) (cm)	6.73
Length (m)	22.86
Weight/length (kg/m)	2.38
Modulus of elasticity (MPa)	13.79
Fracture tension (kN)	13.3
Drogue	
Weight (kg)	29.5
Type (m^2)	0.2322
Reel	
Weight (kg)	68

The calculation of aerodynamic force and restoring force can be seen in Vassberg et al. [20].

3. Improvement of the Take-up System

3.1. Analysis of the Spring-Loaded Take-Up System. The resimulation and analysis of the Reference [20] reveal that the hose internal tension decreases rapidly due to the drag on the drogue counteracted by the push of the probe when they are coupling. And then the slack of the hose happens. Since the adaptive rewinding force provided by the spring-loaded take-up system only depends on the retraction length, it is approximately constant. Its initial value is equal to the steady-state towing force. The towing force, namely, the hose tension at the towing point, sharply dropping at the contact moment, is far less than the rewinding force, and the balance is broken. This imbalance causes an excessive amount of the rewinding (or reel take-up) acceleration calculated from the difference between the rewinding and towing forces, which triggers the excessive take-up phenomenon. The immense rewinding acceleration almost doubles the hose tension and the towing force, and the hose is tightened immediately. Then, the threefold towing force far greater than the rewinding force, in turn, leads to the reel-out instead of the reel-in operation. In the meantime, while the receiver gradually approaches the tanker, the hose slacks again, causing a sharp decrease in its tension. Therefore, the hose tension shows a high-frequency and high-amplitude oscillation when the spring-loaded take-up system works. The tension oscillation of the hose is shown in Figure 3.

3.2. PMSM-RACRL Take-Up System. The above analysis clearly shows that the excessive take-up phenomenon induced by the spring-loaded take-up system is the further reason why the HWP cannot be well suppressed. Therefore, an improved take-up system is proposed to tackle this problem. The PMSM provides the rewinding force of the reel, and the RACRL is added to it. The PMSM has an achievable control of acceleration output, and the RACRL can suppress the excessive take-up phenomenon. The rewinding force is

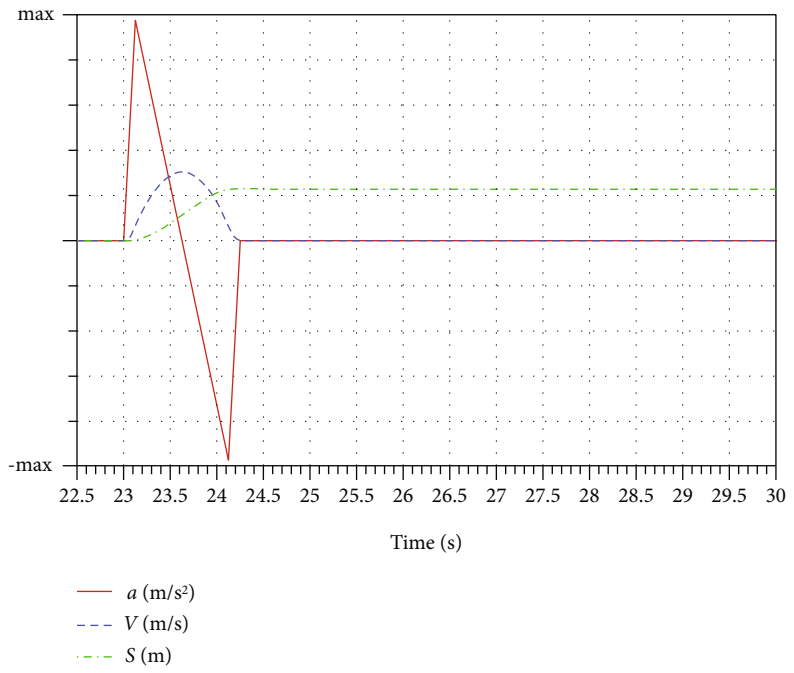

Figure 4: Drogue acceleration, velocity, and displacement characteristics.

Table 3: Cases for the verification.

Case	Restoring force	Reel take-up	a_{max} (m/s^2)	V_{max} (m/s)	T_{total} (s)	Reel a_{max} (m/s^2)	Reel k_{max} (m/s^3)
W1	Yes	No	1.524	0.475	1.25	N/A	N/A
W1E0	No	No	1.524	0.475	1.25	N/A	N/A
W2E0	No	Yes	1.524	0.475	1.25	3.048	N/A
W2E0-k100	No	Yes	1.524	0.475	1.25	3.048	100
W2E0-k1000	No	Yes	1.524	0.475	1.25	3.048	1000
W4aE0-k100	No	Yes	4.877	1.524	1.25	3.048	100
W4aE0-k1000	No	Yes	4.877	1.524	1.25	3.048	1000
W4bE0-k100	No	Yes	4.877	1.524	1.25	N/A	100
W4bE0-k1000	No	Yes	4.877	1.524	1.25	N/A	1000

defined as

$$T_{reel} = T_{static}\left[1 - \frac{s}{L_1}\right], \tag{16}$$

where T_{static} is the maximum towing force of the hose in the steady-state and s is the total length of the hose that has been rewound to the refueling pod. L_1 is the maximum retractable length of the hose during the coupling event, and it is 8.84 m referred from the literature [20].

As the receiver approaches the tanker during the docking event, the hose slacks, resulting in the tension drops. The balance between the rewinding force and the towing force is broken, after which the PMSM take-up system works and retracts the loose hose. So the motion of the reel is described as

$$(T_{reel} - T_{hose})R = I\alpha, \tag{17}$$

where T_{hose} is the real-time tension at the towing point of the hose (N), R is the radius of the drum (m), α is the angular acceleration of the motor (rad/s^2), and I is the moment of inertia of the drum (kg·m^2):

$$I = (M + \rho s)R^2, \tag{18}$$

where M is the mass of the drum (kg), ρ is the dry density of the hose (kg/m), and ρs is the mass of the hose that has been

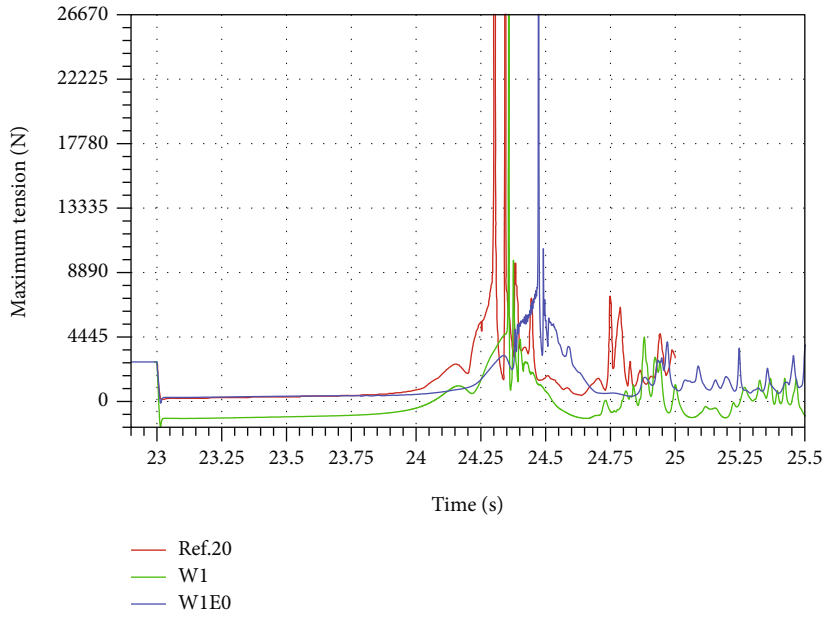

Figure 5: Case W1 tension time history in comparison with Ref. 20.

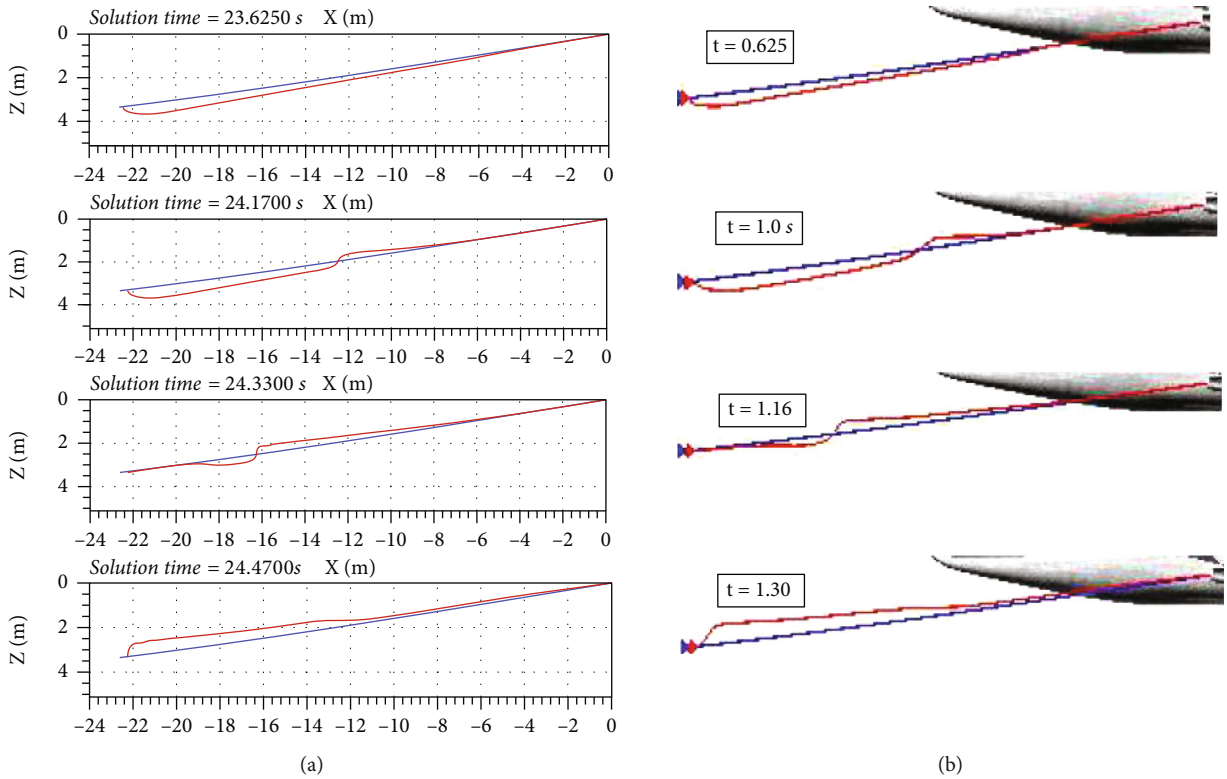

Figure 6: Hose geometry snapshot comparisons of the W1E0 (a) with the Ref. 20 (b).

wrapped around the drum (kg). According to drum radius R and angular acceleration α, the acceleration of the drum to the hose at the towing point can be obtained

$$a = \alpha R. \tag{19}$$

Therefore, under the motor drive, the acceleration of hose reeling in/out may be expressed as

$$a_{\text{reel}} = \frac{T_{\text{reel}} - T_{\text{hose}}}{M + \rho s}. \tag{20}$$

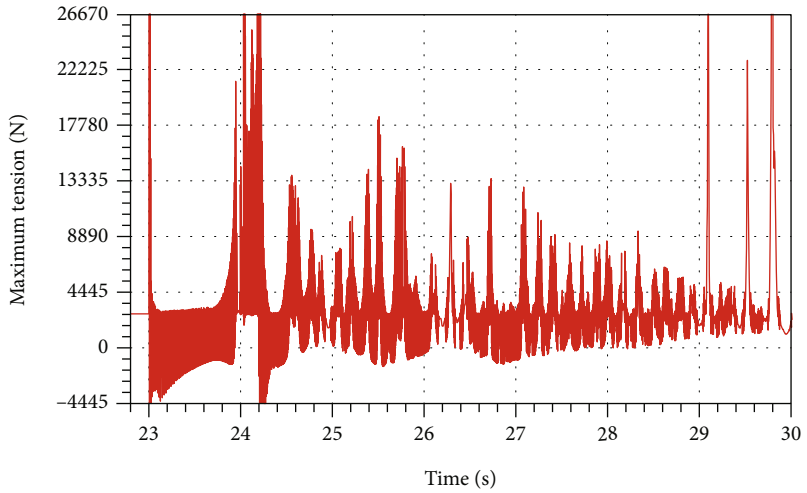

Figure 7: Tension history of case W2E0.

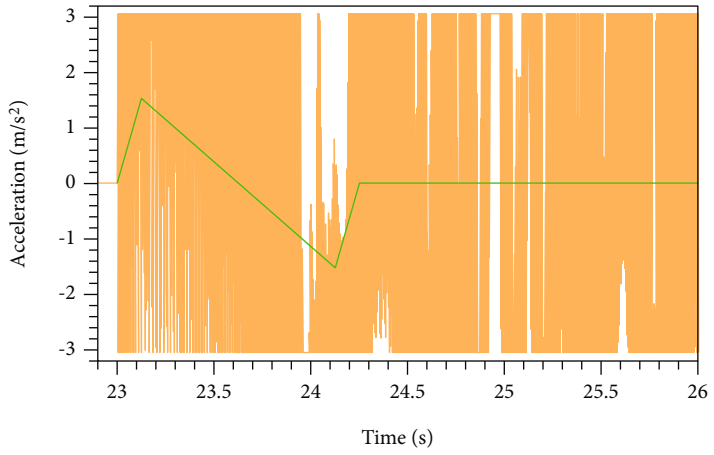

(a) W2E0 acceleration histories in local time

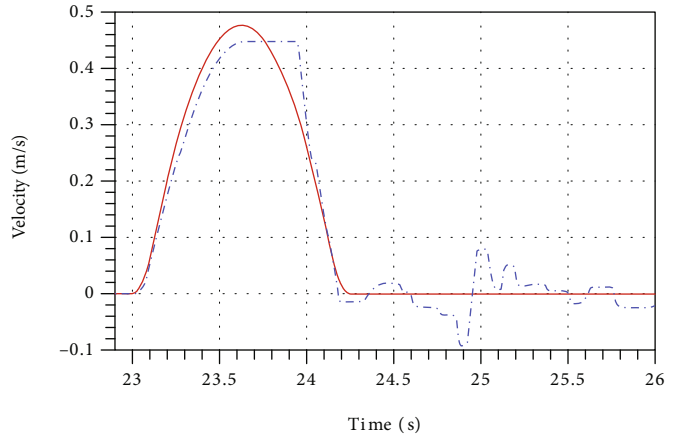

(b) W2E0 velocity histories in local time

Figure 8: W2E0 acceleration and velocity histories.

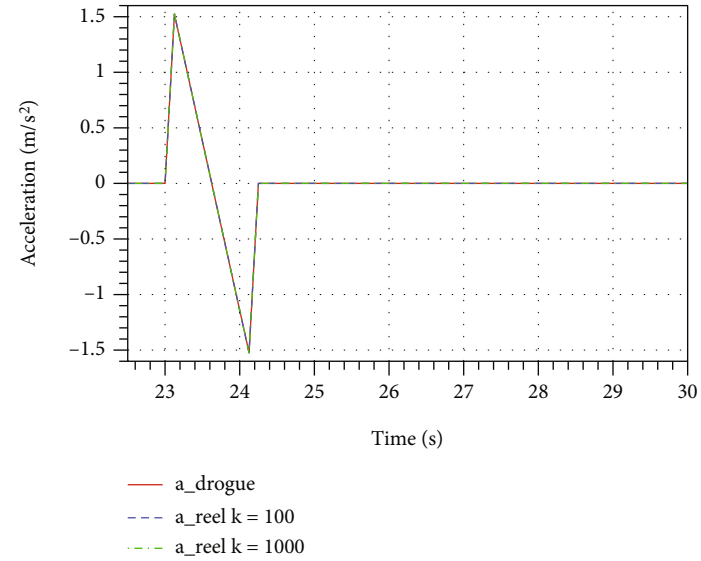

(a) Acceleration histories in global time

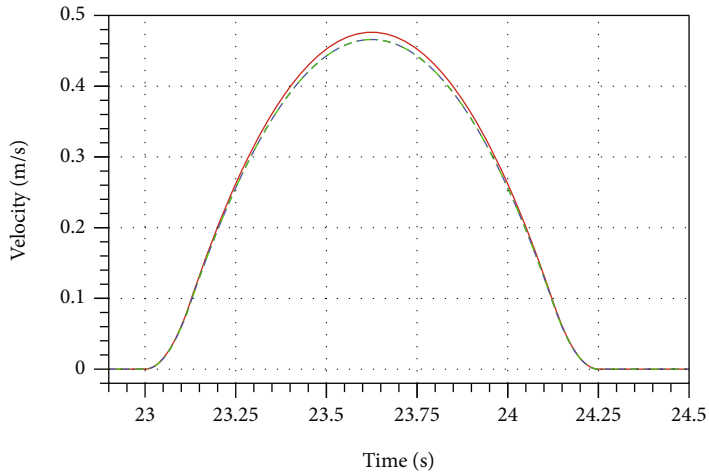

(b) Velocity histories in local time

Figure 9: Case W2E0-k acceleration and velocity histories with different k.

Furthermore, to prevent the excessive take-up phenomenon and tension oscillation, the RACRL is proposed and added:

$$|\dot{a}_{\text{reel}}| \le k, \tag{21}$$

or

$$|\Delta a| \le k\Delta T, \tag{22}$$

where k is the upper limit of the rewinding acceleration changing rate of the hose (m/s^3), and ΔT is the calculation time step. If the limiter is too large, it will lead to overresponse; in turn, too small will lead to underresponse. And $k = 100$ m/s^3 is recommended.

4. Results and Discussions

4.1. Simulation Conditions. The motivation of this paper is to investigate the effectiveness of suppressing HWP by the proposed PMSM-RACRL take-up system. In the current study, only the uniform flow is considered as the background flowfield. The influence of the tanker wake will be addressed in future studies. The physical properties of the hose, drogue, and reel system used in the simulation are referred to Vassberg et al. [20]. The full trailing hose is evenly divided into 200 segments. The uniform flow and physical properties are shown in Tables 1 and 2.

The numerical simulations of suppression HWP have been conducted at various closure accelerations with the PMSM-RACRL take-up system. Before a docking event ($t < 23$ s), the trailing hose-drogue assembly is resting

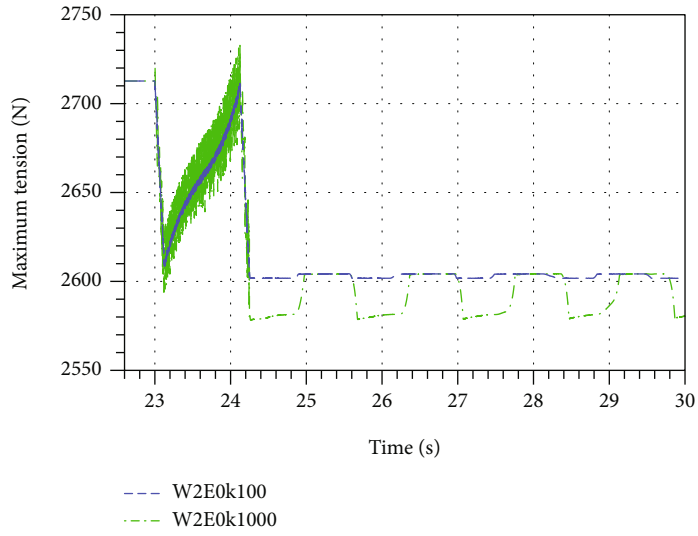

Figure 10: Case W2E0-k tension histories with different k.

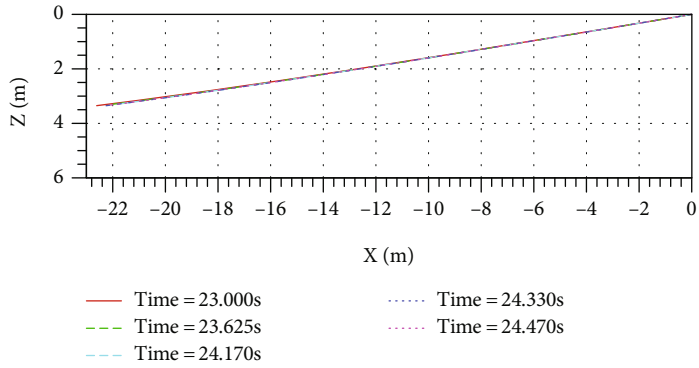

Figure 11: Case W2E0-k100 hose geometry snapshots.

relative to the tanker. And during drogue movement ($23 < t < 24.25$ s), the drogue approaches the tanker with different accelerations after the engagement of the probe. The time histories of drogue acceleration, velocity, and displacement characteristics profiles are shown in Figure 4. To illustrate effectiveness of suppressing HWP by the proposed PMSM-RACRL take-up system at various closure velocity, 9 representative cases are presented in this section, which are summarized in Table 3.

4.2. Maximum $a_{drogue} = 1.524\,m/s^2$ with PMSM-RACRL Reel Take-Up Malfunction (Cases W1 and W1E0). This section is aimed at verifying the accuracy of the adopted finite segment model platform by comparing the current numerical results with those in the literature [20]. Figure 5 shows the tension time histories when the PMSM-RACRL reel take-up system is malfunctioning during hook-up. The red line (Ref. 20) represents the maximum tension of the hose from reference [20], and the green line (W1) and the blue line (W1E0) represent the maximum tension simulated with and without the restoring force, respectively. It shows that after the docking, the green line (W1) is always about 1100 N lower than the red line. Since the drag on the drogue is counteracted when the probe pushes the drogue upstream, the hose is slacking and drooping [15]. However, the restoring force is dealt with as an external force in the existing references, which may lift the drooping hose upwards out of thin air. The lifting action changes the hose from the tensile state to the compression state so that the internal hose tension is further decreased to be negative. It is not reasonable in most situations. On the contrary, the blue line (W1E0) is simulated without the restoring force. It is identical to the literature (Ref. 20) from the beginning of docking (23.0 s) to 23.8 s. Nevertheless, after 23.8 s, the appearance time of tension spike clearly shows that the tension time history of W1E0 existence about 0.17 s delay compared with that of Ref. 20. The lag is caused by the deficiency of the restoring force, delaying the formation of the sine wave. Another evident difference is the tension spike appearance once in W1E0 but twice in Ref. 20, which can be induced by the treatment of restoring force. Besides the lag and the spike's

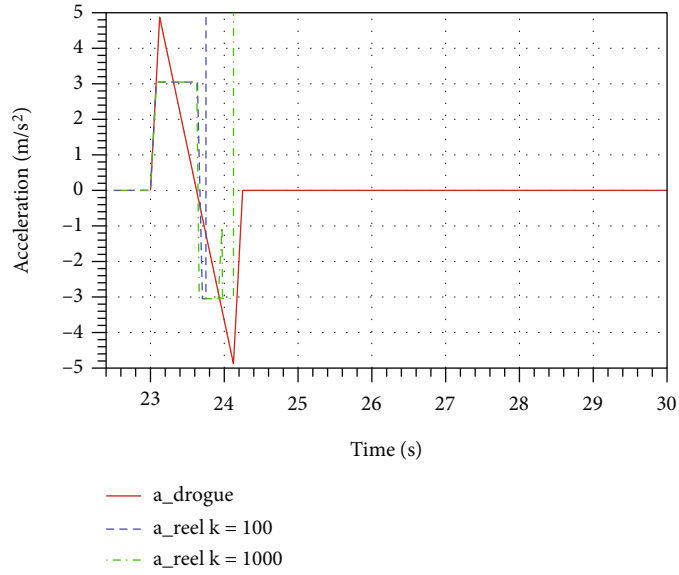

(a) Acceleration histories in global time

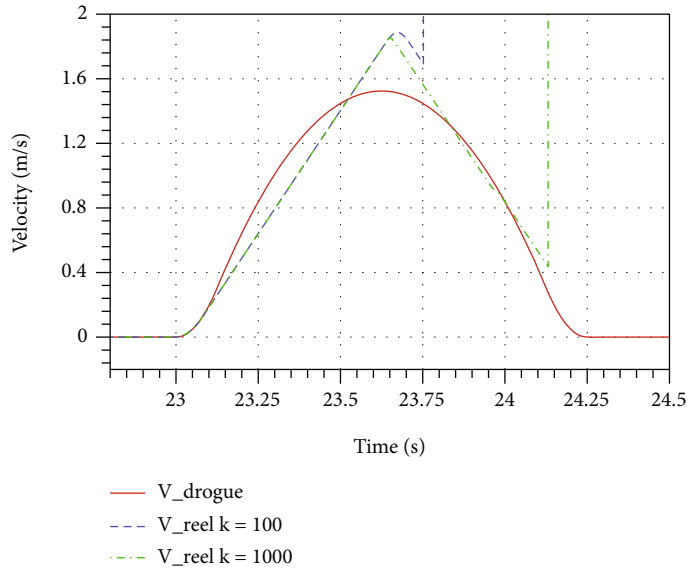

(b) Velocity histories in local time

Figure 12: Case W4aE0-k velocity and acceleration histories with different k.

number, there has little significant difference between the W1E0 and Ref. 20, indicating that the current numerical simulation is reliable.

Figure 6 shows the comparisons of the hose geometry snapshots between the W1E0 (Figure 6(a)) and Ref. 20 (Figure 6(b)). Before the time reaches 23.625 s, the motion of case W1E0 is identical to the literature. However, after 24.17 s, it shows a constant lag of 0.17 s compared with Ref. 20. It demonstrates that the deficient restoring force lags the formation of sine-wave oscillations during $23.625\,\text{s} < t < 24.17\,\text{s}$. And outside of this period, there has little influence on the hose motion. Still, the restoring force does not change the sine-wave oscillations' shape and the propagation speed along with the hose. Considering the restoring force has been treated as an external force is not reasonable, so it is not added in the further verification of PMSM-RACRL reel take-up below.

4.3. Maximum $a_{drogue} = 1.524\,m/s^2$ without RACRL (Case W2E0). To illustrate the indispensable of the RACRL in the reel take-up system when suppressing HWP, case W2E0 is a repeat of W1E0, but this time with only the PMSM reel take-up system engaged (without RACRL). In other words, the limiter k of the PMSM-RACRL reel take-up system is an infinite value. Figure 7 provides the history of the maximum hose tension. At the docking moment ($t = 23$ s), due to the impact of the probe, the hose slacks, and its tension steepest drops suddenly. The reel take-up system starts with a very high rewinding acceleration, triggering the excessive take-up phenomenon. So the next time

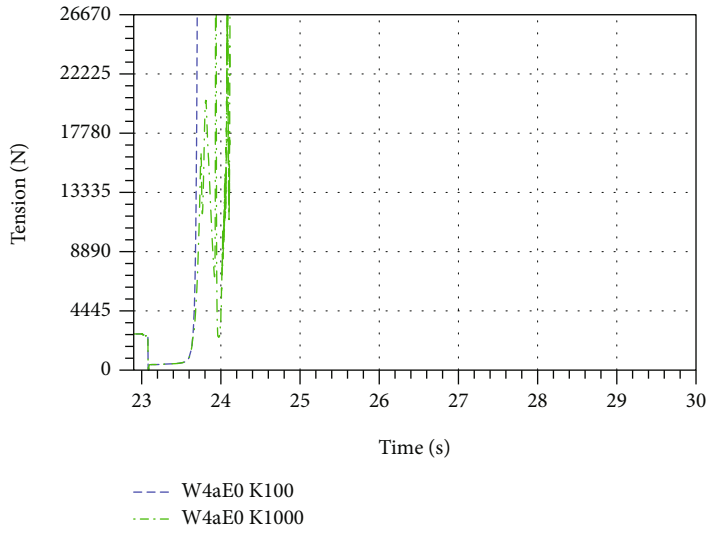

Figure 13: Case W4aE0-k tension histories with different k.

step, the hose tension rebounds to as high as 26670 N. Afterward, the hose tension oscillates in a high frequency, and simultaneously the reel take-up function switches between overresponse and underresponse states. It shows that the hose has experienced intense tension fluctuations during the take-up process. And it tends to converge from 24 to 29 s but eventually diverges.

To further illustrate the importance of RACRL, the motion characteristics of reel and drogue have been analyzed. Figure 8(a) shows that from 23 s to 23.625 s, the reel-in acceleration (positive) is denser than the reel-out acceleration (negative). That is, the overresponse is dominant, so the reel-in speed can still be slowly improved in Figure 8(b). However, from 23.625 s to 23.95 s, the intensities of reel-in/out acceleration are balanced. Therefore, the take-up speed keeps the maximum value of 0.45 m/s. After the drogue has stopped ($t > 24.25$ s), the reel still adjusts its acceleration at a high frequency, indicating that the take-up system has not reached equilibrium and the hose-drogue dynamics are unstable.

The take-up speed slightly lags behind the closure speed from the beginning, indicating that the take-up system is not tightening the hose in time. Though the take-up speed exceeds the closure speed from about 23.75 s to 24.10s, the loose hose has already accumulated a lot of kinetic energy. At this very moment, the take-up system no longer satisfies the inhibition of HWP. The strategy is failed.

According to the tension history in Figure 7, the lag of take-up speed is not caused by the insufficiency of rewinding force but by the continuous fluctuations of hose tension. The oscillations cause the reel to always be in an alternating overresponse and underresponse state, thus impedes the increase in take-up speed. This phenomenon can be demonstrated in Figure 8(a) that the take-up acceleration can easily reach its maximum limit of 3.048 m/s^2 proves that the rewinding force is sufficient.

4.4. Maximum $a_{drogue} = 1.524$ m/s^2 with RACRL (Cases W2E0-k100 and W2E0-k1000). To illustrate the effect of RACRL in the reel take-up system and the impact of its value on the hose dynamics, cases W2E0-k100 and W2E0-k1000 are repeat of case W2E0, but with additional RACRL engaged. Figure 9 shows the time histories of the accelerations and velocities at the drogue and reel ($k = 100$ and $k = 1000$) sides, respectively. During coupling, the acceleration curves of the drogue and reel are coincident in Figure 9(a). And in Figure 9(b), the take-up speeds are nearly synchronized with the drogue speed. In other words, the take-up system responds timely and felicitously, and no loosening occurs all the time. Compared with W2E0, W2E0-k demonstrates a significant improvement of the take-up system with the additional RACRL.

Figure 10 provides the histories of the maximum hose tension of cases W2E0-k100 and W2E0-k1000, respectively. During drogue movement, their tension oscillation range is from 2560 to 2740 N, significantly improving over -4445 to 26670 N of case W2E0 in Figure 7. Afterward, the drogue and the tanker are relatively stationary, and the hose tension oscillates regularly and slightly. The tension oscillation in the docking process has been incredibly well controlled with the addition of the RACRL. Therefore, the W2E0-k tension histories suggest that the RACRL is the key to the success of HWP suppression.

Furthermore, during drogue movement, the green line completely covers the blue line, indicating that the amplitude of tension oscillation is positively correlated with the value of k.

Figure 11 shows the hose geometry snapshots of case W2E0-k100 during the docking event. The hose geometry snapshots are nearly overlapping in different time histories, and no significant sine-wave oscillations have been observed. It demonstrates that the hose is retracted calmly during the drogue movement.

4.5. Maximum $a_{drogue} = 4.877$ m/s^2 with RACRL (Cases W4aE0-k100 and W4aE0-k1000). To illustrate the PMSM-RACRL reel take-up system response when beyond normal operating conditions, an excessive closure acceleration

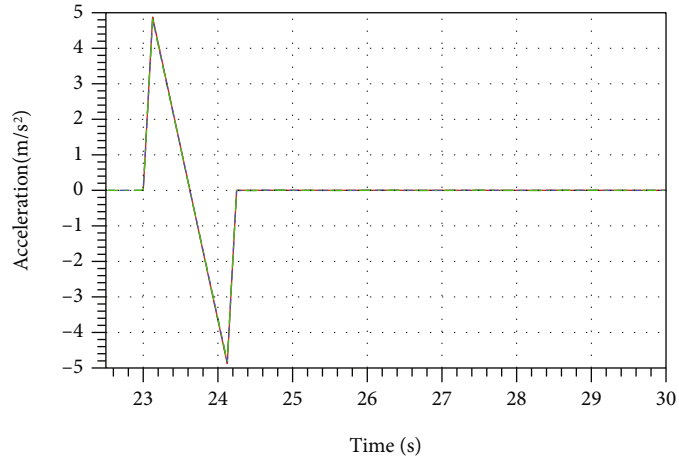

(a) Acceleration histories in global time

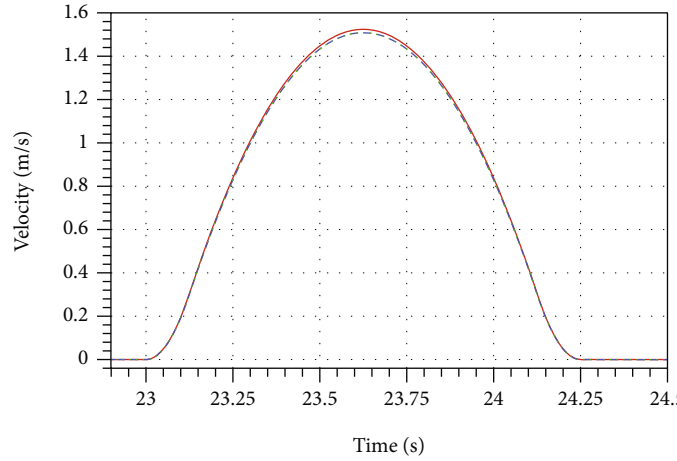

(b) Velocity histories in local time

FIGURE 14: Case W4bE0-k velocity and acceleration histories with different k.

$a_{\text{drogue}} = 4.877\ \text{m/s}^2$ is used. Figure 12 shows the acceleration and velocity histories of the drogue and reel, respectively. Since the maximum closure acceleration of the drogue ($4.877\ \text{m/s}^2$) is greater than the maximum rewinding acceleration of the reel take-up systems ($3.048\ \text{m/s}^2$), the take-up accelerations are limited to their maximum during $23.078 < t < 23.75$ s ($k = 100$) and $23.078 < t < 24.14$ s ($k = 1000$), respectively, in Figure 12(a). And in Figure 12(b), the take-up speed curves are straight lines, and they are smaller than the closure speed during the period $23.078 < t < 23.52$ s. So it is inevitable that the hoses are slacking. Finally, the whipping happens at 23.75 s ($k = 100$) and 24.125 s ($k = 1000$), respectively.

Figure 13 shows the tension histories of case W4aE0-k. Since the reel acceleration is limited after 23.078 s, the rewinding speed lags behind the drogue velocity, leading the reel take-up system to lose its capability to tighten the hose. During $23.078\ \text{s} < t < 23.6$ s, their tension curves are similar to that of case W1E0, in which the reel take-up system is malfunctioning. Case W4aE0-k demonstrates that the take-up system is normal working; as long as the maximum take-up acceleration is lower than the maximum closure acceleration, the HWP still happens, with tension spikes exceed the hose fracture value.

4.6. Maximum $a_{drogue} = 4.877\ \text{m/s}^2$ with RACRL (Cases W4bE0-k100 and W4bE0-k1000). To illustrate the effectiveness of the PMSM-RACRL reel take-up system with an excessive closure acceleration, W4bE0-k are repeat of W4aE0-k, but without the maximum reel acceleration limit. Figure 14 shows the

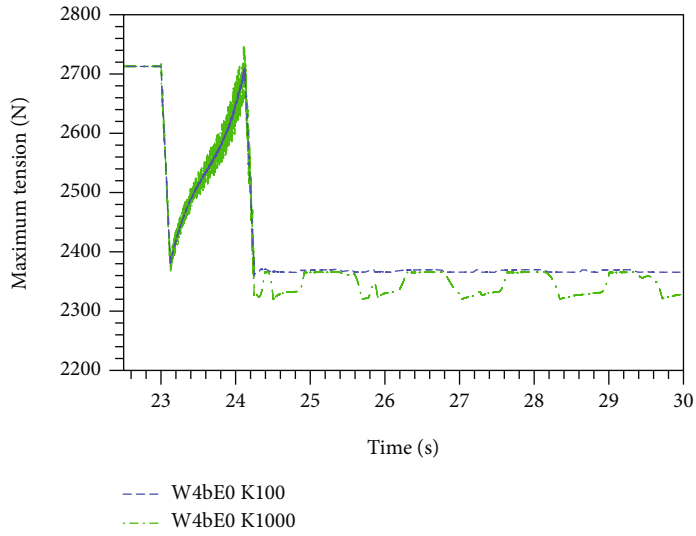

Figure 15: Case W4bE0-k tension histories with different k.

velocity and acceleration histories with different k. During the coupling, the reel take-up accelerations and speeds follow very well with the closure acceleration and speed, respectively. As a result, the hose is retracted in a steady state, and no significant slack forms.

Figure 15 shows the tension histories of case W4bE0-k. During drogue movement, their tension oscillation range is from 2340 to 2740 N, similar to case W2E0-k. It demonstrates that even the engagement acceleration is excessive, the PMSM-RACRL reel take-up system can timely and effectively work when without the maximum reel acceleration limit. The hose dynamics and the hose tension are controlled, and the HWP is completely suppressed.

Like case W2E0-k, the green line ($k = 1000\ \mathrm{m/s^3}$) entirely covered the blue line ($k = 100\ \mathrm{m/s^3}$) during the drogue movement. It reveals that the greater the k value, the weaker the hose tension oscillation is controlled.

5. Conclusions

The spring-loaded reel take-up system is analyzed, and an improved PMSM-RACRL reel take-up system is proposed. The numerical results are summarized in the following:

(1) It is the oscillation of hose tension, not the insufficiency of rewinding force, which prevents the take-up speed following up the closure speed

(2) The maximum rewinding acceleration of the reel take-up system should not be smaller than the maximum closure acceleration of the drogue. Otherwise, it will inevitably lead the reel take-up speed to lag behind the closure velocity, and then the hose slack and whipping

(3) The $k = 100\ \mathrm{m/s^3}$ is recommended to RACRL. Too small may lead to the underresponse of the reel, while too large may weaken the control of tension oscillations, even result in the RACRL is not working

(4) The new PMSM-RACRL reel take-up system accomplishes the active control of tension oscillation and suppressing HWP with a straightforward strategy within and beyond normal operating conditions. The amplitude of tension oscillation is reduced to one-tenth of that without active control

Data Availability

The data that support the findings of this study are available from the corresponding author upon reasonable request.

Conflicts of Interest

The authors declared no potential conflicts of interest with respect to the research, authorship, and/or publication of this article.

References

[1] M. Ownby, "Mixed initiative control of automa-teams (MICA) - a progress Report," in *AIAA 3rd "unmanned Unlimited" Technical Conference, Workshop and Exhibit*, pp. 20–23, Chicago, Illinois, 2004.

[2] E. Wyatt, "The DARPA/air force unmanned combat air vehicle (UCAV) program," in *AIAA international air and space symposium and exposition: the next 100 years*, pp. 14–17, Dayton, Ohio, 2003.

[3] K. Ro, H. Ahmad, and J. W. Kamman, "Dynamic modeling and simulation of hose-paradrogue assembly for mid-air operations," in *AIAA infotech @ aerospace conference*, pp. 6–9, Seattle, Washington, 2009.

[4] J. P. Nalepka and J. L. Hinchman, "Automated aerial refueling: extending the effectiveness of UAVs," in *AIAA Modeling & Simulation Technologies Conference and Exhibit*, pp. 15–18, San Francisco, CAL, 2005.

[5] P. Thomas, P. R. Thomas, and P. R. Thomas, "Bow wave effect in probe and drogue aerial refueling," in *AIAA Guidance, Navigation, and Control (GNC) Conference*, Boston, MA, 2013.

[6] C. McFarlane, *An Investigation of Flying Qualities for Fixed Wing Unmanned Aerial Vehicles*, University of Bristol, 2009.

[7] R. P. Dibley, M. J. Allen, and N. Nabaa, "Autonomous airborne refueling demonstration, phase I flight-test results," in *AIAA Atmospheric Flight Mechanics Conference and Exhibit*, Hilton head, South Carolina, 2007.

[8] Z. Liu, J. Liu, and W. He, "Modeling and vibration control of a flexible aerial refueling hose with variable lengths and input constraint," *Automatica*, vol. 77, pp. 302–310, 2017.

[9] Y. T. Choi and N. M. Werele, "Semi-active magnetorheological refueling probe systems for aerial refueling events," *Smart Materials and Structures*, vol. 22, no. 9, p. 092001, 2013.

[10] T. Kuk, "Active control of aerial refueling drogue," *Western Michigan University*, pp. 5-6, 2014.

[11] J. L. Hansen, J. E. Murray, and N. V. Campos, "The NASA dryden AAR project: a flight test approach to an aerial refueling system," in *AIAA Atmospheric Flight Mechanics Conference*, 2004.

[12] K. Ro and J. W. Kamman, "Modeling and simulation of hose-paradrogue aerial refueling systems," *Journal of Guidance, Control, and Dynamics*, vol. 33, no. 1, pp. 53–63, 2010.

[13] Z. H. Zhu and S. A. Meguid, "Elastodynamic analysis of aerial refueling hose using curved beam element," *AIAA Journal*, vol. 44, no. 6, pp. 1317–1324, 2006.

[14] K. Ro, T. Kuk, and J. W. Kamman, "Active control of aerial refueling hose-drogue systems," in *AIAA Guidance, Navigation, and Control Conference*, Toronto, Ontario Canada, 2010.

[15] K. Ro, T. Kuk, and J. W. Kamman, "Dynamics and control of hose-drogue refueling systems during coupling," *Journal of Guidance, Control, and Dynamics*, vol. 34, no. 6, pp. 1694–1708, 2011.

[16] W. R. Gates and M. J. McCarthy, "United States Marine Corps aerial refueling requirements analysis," in *Simulation Conference Proceedings*, Winter, 2000.

[17] J. Vassberg, D. Yeh, A. J. Blair, and J. Evert, "Dynamic characteristics of a KC-10 wing-pod refueling hose by numerical simulation," in *20th AIAA applied aerodynamics conference*, St. Louis, Missouri, 2002.

[18] A. Styuart, R. Gaston, H. Yamashiro, R. Stirling, and M. Mor, "Numerical simulation of hose whip phenomenon in aerial refueling," in *AIAA Atmospheric Flight Mechanics Conference*, Portland, Oregon, 2011.

[19] W. Ribbens, F. Saggio, R. Wierenga, and M. Feldmann, "Dynamic modeling of an aerial refueling hose & drogue system," in *25th AIAA applied aerodynamics conference*, Miami, FL, 2007.

[20] J. Vassberg, D. Yeh, A. J. Blair, and J. Evert, "Numerical simulations of KC-10 wing-mount aerial refueling hose-drogue dynamics with a reel take-up system," in *21st AIAA Applied Aerodynamics Conference*, Orlando, Florida, 2003.

[21] J. Vassberg, D. Yeh, A. J. Blair, and J. Evert, "Numerical simulations of KC-10 centerline aerial refueling hose-drogue dynamics with a reel take-up system," in *22nd AIAA Applied Aerodynamics Conference and Exhibit*, Providence, Rhode Island, 2004.

[22] J. Vassberg, D. Yeh, A. Blair, and J. Evert, "Numerical simulations of KC-10 in-flight refueling hose-drogue dynamics with an approaching F/A-18D receiver aircraft," in *AIAA Applied Aerodynamics Conference*, Toronto, Ontario Canada, 2005.

[23] H. T. Wang, X. M. Dong, J. P. Xue, and J. Liu, "Dynamic modeling of a hose-drogue aerial refueling system and integral sliding mode backstepping control for the hose whipping phenomenon," *Chinese Journal of Aeronautics*, vol. 27, no. 4, pp. 930–946, 2014.

[24] Z. Su, M. Xie, and C. Li, "RISE based active vibration control for the flexible refueling hose," *Aerospace Science and Technology*, vol. 92, pp. 387–404, 2019.

[25] W. H. Zhang, X. L. Shao, W. D. Zhang, J. Qi, and H. Li, "Unknown input observer-based appointed-time funnel control for quadrotors," *Aerospace Science and Technology*, vol. 126, no. 7, p. 107351, 2022.

[26] X. L. Shao, J. T. Zhang, and W. D. Zhang, "Distributed Cooperative Surrounding Control for Mobile Robots with Uncertainties and Aperiodic Sampling," *IEEE Transactions on Intelligent Transportation Systems*.